JGR Atmospheres

RESEARCH ARTICLE
10.1029/2019JD030945

Analysis of the Spatial Nonuniformity of the Electric Field in Spectroscopic Diagnostic Methods of Atmospheric Electricity Phenomena

A. Malagón-Romero[1], F. J. Pérez-Invernón[1], A. Luque[1], and F. J. Gordillo-Vázquez[1]

[1]Instituto de Astrofísica de Andalucía (IAA), CSIC, Granada, Spain

Key Points:
- The spatial nonuniformity of the electric field in streamer discharges affects the estimation of the peak electric field value
- We present two diagnostic methods to estimate the peak electric field in streamer heads at different pressures
- We analyze the optical emissions measured by Armstrong et al. during SPRITE's 1995 and 1996 campaigns

Correspondence to:
A. Malagón-Romero,
amaro@iaa.es

Citation:
Malagón-Romero, A., Pérez-Invernón, F. J., Luque, A., & Gordillo-Vázquez, F. J. (2019). Analysis of the spatial nonuniformity of the electric field in spectroscopic diagnostic methods of atmospheric electricity phenomena. *Journal of Geophysical Research: Atmospheres*, *124*, 12,356–12,370. https://doi.org/10.1029/2019JD030945

Received 3 MAY 2019
Accepted 5 SEP 2019
Accepted article online 12 SEP 2019
Published online 28 NOV 2019

Abstract The spatial nonuniformity of the electric field in air discharges, such as streamers, can influence the accuracy of spectroscopic diagnostic methods and hence the estimation of the peak electric field. In this work, we use a self-consistent streamer discharge model to investigate the spatial nonuniformity in streamer heads and streamer glows. We focus our analysis on air discharges at atmospheric pressure and at the low pressure of the mesosphere. This approach is useful to investigate the spatial nonuniformity of laboratory discharges as well as sprite streamers and blue jet streamers, two types of transient luminous events taking place above thunderclouds. This characterization of the spatial nonuniformity of the electric field in air discharges allows us to develop two different spectroscopic diagnostic methods to estimate the peak electric field in cold plasmas. The commonly employed method to derive the peak electric field in streamer heads underestimates the electric field by about 40–50% as a consequence of the high spatial nonuniformity of the electric field. Our diagnostic methods reduce this underestimation to about 10–20%. However, our methods are less accurate than previous methods for streamer glows, where the electric field is uniformly distributed in space. Finally, we apply our diagnostic methods to the measured optical signals in the second positive system of N_2 and the first negative system of N_2^+ of sprites recorded by Armstrong et al. (1998, https://doi.org/10.1016/S1364-6826(98)00026-1) during the SPRITE's 1995 and 1996 campaigns.

1. Introduction

Nonequilibrium (or nonthermal) air discharges are due to the application of an electric field, which provides energy to the electrons and maintains the ionization of air molecules. In nonequilibrium discharges, the electron temperature exceeds the background temperature. The discharge parameters that determine the type of discharge are their spatial and temporal scales, the production of electron avalanches, and the plasma and air temperature. We refer to Bruggeman et al. (2017) for a detailed description of the different types of nonthermal air discharges.

Nonequilibrium air discharges have numerous industrial applications (Šimek, 2014) and are closely related to atmospheric electricity phenomena, such as lightning and transient luminous events (TLEs; Franz et al., 1990; Pasko et al., 2012). TLEs are upper atmospheric discharges related to lightning. Sprites and blue jets are TLEs that occur above thunderstorms that cover altitudes ranging between 20 and 85 km (Gordillo-Vázquez & Donkó, 2009; Gordillo-Vázquez et al., 2018; Pasko et al., 1996; Stenbaek-Nielsen et al., 2000; Wescott et al., 1995, 1996, 1998, 2001). The lower part of sprites and the upper part of blue jets are formed by hundreds of streamer discharges (Kuo et al., 2015; Luque et al., 2016; Parra-Rojas et al., 2014) and emit light predominantly in some band systems of molecular nitrogen. Sprites are one of the largest nonthermal air discharges in nature. For a more extensive review of TLEs and sprites, we refer to Pasko et al. (2012).

Gallimberti et al. (1974) and Goldman and Goldman (1978, p. 243) investigated the optical spectra of air corona discharges at atmospheric pressure, noting that the spectra were dominated by N_2 emissions. Later investigations (see Kondo and Ikuta, 1980; Stritzke et al., 1977 and references collected by Šimek, 2014) confirmed that nonequilibrium air discharges emit light predominantly in the first and second positive band systems of the molecular neutral nitrogen (1PS N_2 and the 2PS N_2, or simply FPS and SPS), the first negative band system of the molecular nitrogen ion (N_2^+-1NS or simply FNS), the Meinel band system of the molecular nitrogen ion (Meinel N_2^+), and the Lyman-Birge-Hopfield band system of the molecular neutral nitrogen. In

this work, we will refer to FNS, FPS, and SPS for the sum of optical emissions between all the vibrational states. The emissions from the vibrational state $v' = v_i$ to all v'' will be labeled as $FNS_{(v_i,v'')}$, $FPS_{(v_i,v'')}$, and $SPS_{(v_i,v'')}$. Finally, the emissions from the vibrational state $v' = v_i$ to $v'' = v_j$ will be labeled as $FNS_{(v_i,v_j)}$, $FPS_{(v_i,v_j)}$, and $SPS_{(v_i,v_j)}$.

The electronic excitation thresholds for the production of $N_2(B^3\Pi_g, v = 0)$, $N_2(C^3\Pi_u, v = 0)$, and $N_2^+(B^2\Sigma_u^+, v = 0)$ are respectively 7.35, 11.03, and 18.80 eV (Phelps & Pitchford, 1985). Therefore, the population of these emitting molecules in air discharges depends on the electric field that provides energy to the electrons. Excited molecules $N_2(B^3\Pi_g, v = 0)$, $N_2(C^3\Pi_u, v = 0)$, and $N_2^+(B^2\Sigma_u^+, v = 0)$ can respectively emit photons in the optical FPS, SPS, and FNS. Creyghton (1994) proposed the use of the intensity ratio of FNS to SPS to estimate the peak electric field that produces these molecular excitation in streamers. Other authors have also used this intensity ratio to estimate the peak electric field in air discharges (Adachi et al., 2006; Bonaventura et al., 2011; Celestin & Pasko, 2010; Hoder et al., 2012, 2016; Kim et al., 2003; Kozlov et al., 2001; Kuo et al., 2009, 2013, 2005; Liu et al., 2006; Morrill et al., 2002; Paris et al., 2004, 2005; Pasko, 2010; Shcherbakov & Sigmond, 2007). The ratio of FPS to SPS has also been proposed to calculate the peak electric field in air discharges (Šimek, 2014). Ihaddadene and Celestin (2017) proposed a spectroscopic diagnostic method to derive the altitude of sprites streamers based on the altitude dependence of the quenching rate of different electronic excited states of N_2.

Creyghton (1994) and Naidis (2009) noted that the peak electric field obtained from the ratio of FNS to SPS in streamer discharges is distorted by the spatial nonuniformity of the streamer head. Celestin and Pasko (2010) used a self-consistent streamer model to calculate the synthetic optical emissions of positive and negative streamers. They compared the peak electric field calculated by the model with the peak electric field estimated from the synthetic optical emissions. According to Celestin and Pasko (2010), the peak electric field obtained from the ratio of FNS to SPS in streamer discharges must be multiplied by a factor Γ_E ranging between 1.4 and 1.5.

Apart from the spatial nonuniformity of the streamer discharge, the uncertainty of the reaction rates involved in the discharge can lead to a significant error in the estimated electric field (Creyghton, 1994; Hoder et al., 2016; Kozlov et al., 2001; Paris et al., 2004). Recently, Obrusnik et al. (2018) and Bílek et al. (2018) performed a sensitivity analysis to determine the effect of the reaction rate uncertainties in the obtained peak electric field at different pressures using the ratio of FNS to SPS. According to their results, the processes that significantly influence the error in the estimated peak electric field from optical emissions are the excitation by electron impact, the radiative de-excitation, and the electronic quenching by air of electronically excited states of N_2 and N_2^+, especially at atmospheric pressure. Šimek (2014) reported an additional error in the estimated peak electric field from the ratio of FPS to SPS as a consequence of the electric field dependence of the vibrational distribution function of $N_2(B^3\Pi_g, v')$ at relatively low electric field values (~150–200 Td). Finally, Šimek (2014) and Pérez-Invernón, Luquen, Gordillo-Vazquez, Sato, et al. (2018) demonstrated that the ratio of FPS to SPS is highly inaccurate for reduced electric field values above ~200 Td, as this ratio is almost electric field independent for higher electric field values.

In this work, we develop two methods to reduce the uncertainty in the estimated peak electric field caused by the spatial nonuniformity of the discharge using the ratio of FNS to SPS and FPS to SPS. First, we use a streamer model to calculate the synthetic optical emissions of a laboratory streamer head, a sprite streamer head, and a sprite streamer glow. By sprite streamer glow we refer to the column-like luminous structure that appears in the sprite streamer wake after the streamer head passage (Gordillo-Vázquez & Luque, 2010; Liu, 2010; Luque & Ebert, 2010; Luque et al., 2016; Stenbaek-Nielsen & McHarg, 2008). Second, we use the model to analyze the nonuniformity of the discharges. Finally, we use the synthetic optical emissions and the spatial nonuniformity of the discharges to make more accurate the commonly used method to calculate the peak electric field in the plasma.

The organization of this paper is as follows: Section 2 briefly describes the streamer model used to generate the synthetic optical emissions of streamer heads and a glow. Sections 3 and 4 are devoted to the improved diagnostic methods for nonuniform air discharges. Section 5 highlights the applicability of the methods in the analysis of optical emissions from TLEs reported by Armstrong et al. (1998). The conclusions are finally presented in section 6.

Table 1
Most Important Processes for the Optical Emissions

Chemical reaction	Rate	Reference
$e + N_2(X^1\Sigma_g^+, v = 0) \rightarrow N_2^+(B^2\Sigma_u^+, v' = 0) + 2e$	$k_{B^2\Sigma_u^+,0} = f\left(\frac{E}{N}\right)$	Hagelaar and Pitchford (2005); Phelps and Pitchford (1985)
$e + N_2(X^1\Sigma_g^+, v = 0) \rightarrow N_2^+(B^2\Sigma_u^+, v' = 1) + 2e$	$k_{B^2\Sigma_u^+,1} = f\left(\frac{E}{N}\right)$	Hagelaar and Pitchford (2005); Phelps and Pitchford (1985)
$e + N_2(X^1\Sigma_g^+, v = 0) \rightarrow N_2(B^3\Pi_g, v') + e$	$k_{B^3\Pi_g} = f\left(\frac{E}{N}\right)$	Hagelaar and Pitchford (2005); Phelps and Pitchford (1985)
$e + N_2(X^1\Sigma_g^+, v = 0) \rightarrow N_2(C^3\Pi_u, v') + e$	$k_{C^3\Pi_u} = f\left(\frac{E}{N}\right)$	Hagelaar and Pitchford (2005); Phelps and Pitchford (1985)
$N_2^+(B^2\Sigma_u^+, v' = 0) \rightarrow N_2^+(X^2\Sigma_g^+, v'' = 0) + h\nu(\mathrm{FNS}_{(0,v'')})$	$A_{B^2\Sigma_u^+(0,v'')} = 1.14 \times 10^7\ \mathrm{s}^{-1}$	Gilmore et al. (1992)
$N_2^+(B^2\Sigma_u^+, v' = 1) \rightarrow N_2^+(X^2\Sigma_g^+, v'' = 0) + h\nu(\mathrm{FNS}_{(1,v'')})$	$A_{B^2\Sigma_u^+(1,v'')} = 3.71 \times 10^6\ \mathrm{s}^{-1}$	Gilmore et al. (1992)
$N_2(B^3\Pi_g, v') \rightarrow N_2(X^1\Sigma_g^+, v'') + h\nu(\mathrm{FPS})$	$A_{B^3\Pi_g} = 1.34 \times 10^5\ \mathrm{s}^{-1}$	Capitelli et al. (2000)
$N_2(C^3\Pi_u, v') \rightarrow N_2(B^3\Pi_g, v'') + h\nu(\mathrm{SPS})$	$A_{C^3\Pi_u} = 2.47 \times 10^7\ \mathrm{s}^{-1}$	Capitelli et al. (2000)
$N_2^+(B^2\Sigma_u^+, v = 0) + M \rightarrow N_2^+(X^2\Sigma_g^+, v = 0) + M$	$Q_{B^2\Sigma_u^+,N_2} = 8.84 \times 10^{-10}\ \mathrm{cm}^3/\mathrm{s}$, $Q_{B^2\Sigma_u^+,O_2} = 10.45 \times 10^{-10}\ \mathrm{cm}^3/\mathrm{s}$	Dilecce et al. (2010)
$N_2^+(B^2\Sigma_u^+, v = 1) + M \rightarrow N_2^+(X^2\Sigma_g^+, v = 0) + M$	$Q_{B^2\Sigma_u^+,N_2} = 16 \times 10^{-10}\ \mathrm{cm}^3/\mathrm{s}$, $Q_{B^2\Sigma_u^+,O_2} = 10.45 \times 10^{-10}\ \mathrm{cm}^3/\mathrm{s}$	Jolly and Plain (1983)
$N_2(B^3\Pi_g, v) + M \rightarrow$ Deactivated products	$Q_{B^3\Pi_g,N_2} = 2 \times 10^{-12}\ \mathrm{cm}^3/\mathrm{s}$, $Q_{B^3\Pi_g,O_2} = 3 \times 10^{-10}\ \mathrm{cm}^3/\mathrm{s}$	Capitelli et al. (2000)
$N_2(C^3\Pi_u, v) + M \rightarrow$ Deactivated products	$Q_{C^3\Pi_u,N_2} = 10^{-11}\ \mathrm{cm}^3/\mathrm{s}$, $Q_{C^3\Pi_u,O_2} = 3 \times 10^{-10}\ \mathrm{cm}^3/\mathrm{s}$	Capitelli et al. (2000)

2. Streamer Model

Our model is 2D cylindrically symmetric, and the dynamics of all charged species is described by diffusion-drift-reaction equations for electrons and ions coupled with Poisson's equation as follows:

$$\frac{\partial n_e}{\partial t} = \nabla \cdot \left(n_e \mu_e \mathbf{E} + D_e \nabla n_e\right) + C_e + S_{ph}, \tag{1a}$$

$$\frac{\partial n_i}{\partial t} = C_i + S_{ph}, \tag{1b}$$

$$-\nabla \cdot \mathbf{E} = \nabla^2 \phi = -\frac{\rho}{\epsilon_0}, \tag{1c}$$

where $n_{e,i}$ is the number density for electrons and ions, respectively, μ_e is the electron mobility, and D_e is the diffusion coefficient. In the present model, we consider ions motionless over the short time scales that we study, and therefore, we neglect mobility and diffusion coefficients of ions. The term $C_{s=e,i}$ is the net production of species s due to chemical processes, and S_{ph} is the photoionization term that we calculate following the procedure described by Luque et al. (2007). Photoionization acts only on the densities of e and O_2^+. As for Poisson's equation, E is the electric field, ϕ is the electrostatic potential, ρ is the density of charges, and ϵ_0 is the permittivity of vacuum. In this work, we use the local field approximation, and therefore, transport coefficients are derived from the electron energy distribution function that depends only on the local electric field.

The streamers develop in a N_2:O_2 mixture (79:21), and the basic kinetic scheme accounts for impact ionization and attachment/detachment, as described in the supplementary material by Luque et al. (2017), but excluding the water chemistry. Some of the collisions that the electrons undergo excite molecules electronically and vibrationally. These excited molecules either decay emitting a photon of a given frequency or are collisionally quenched, that is, decay to a fundamental level through collisions with N_2 and O_2. In order to account for these emissions, we include electronic and vibrational excitations and de-excitations as well as radiative decay and quenching. Table 1 summarizes the most important processes that influence the optical emissions.

Finite volume methods are suitable to solve the set of equations (1). To solve these equations, we have used CLAWPACK/PETCLAW (Alghamdi et al., 2011; Clawpack Development Team, 2017; LeVeque, 2002). PETCLAW is built upon PETSc (Balay, 2016; Balay et al., 2016) and allows us to split the simulation domain

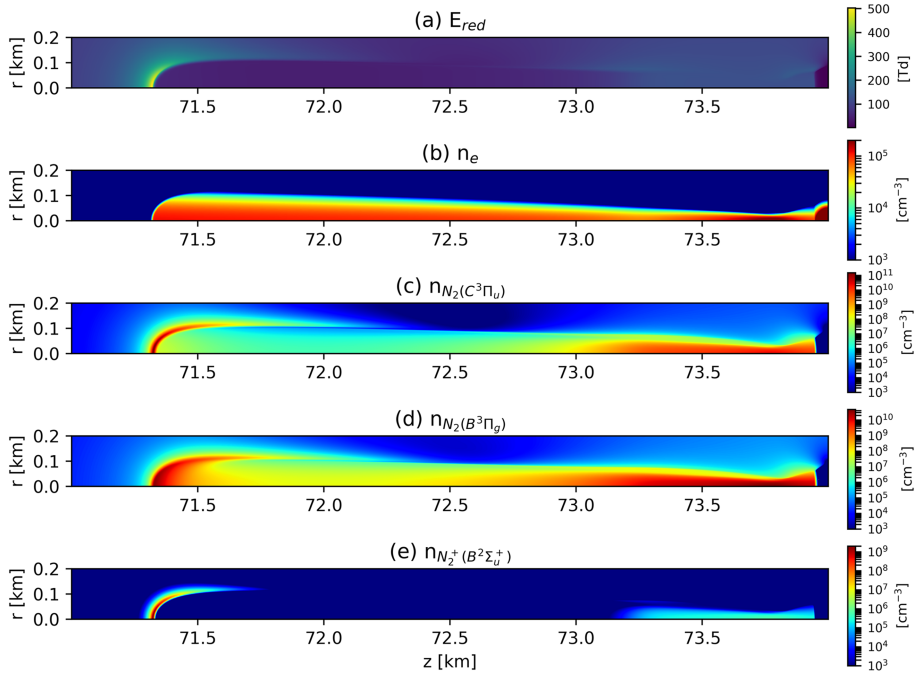

Figure 1. Cross-sectional view of (a) reduced electric field, (b) electron density, and (c–e) density of emitting molecules for a downward propagating positive sprite streamer and a glow for a background electric field of 100 V/m at time 0.9 ms.

into different subdomains (problems) that can be solved in parallel. Poisson's equation is solved using the generalized minimal residual method and the geometric algebraic multigrid preconditioner, both from the PETSc numerical library.

2.1. Sprite Streamer

Sprites are high-altitude discharges made of many streamers that propagate through a varying air density. In our model, the air density follows a decaying exponential profile with an *e*-folding length of 7.2 km. We also set a background electron density following the Wait-Spies profile:

$$n_{\mathrm{e,bg}} = \left(10^4 \mathrm{m}^{-3}\right) \times e^{-(z-60\,\mathrm{km})/2.86\,\mathrm{km}}. \tag{2}$$

In order to start the streamer, we set a gaussian seed with an *e*-folding radius of 20 m and a peak density of $5 \times 10^{12} \mathrm{m}^{-3}$. This initial electron density is neutralized by an identical density of positive ions. In order to solve Poisson's equation, we impose Dirichlet boundary conditions at $z = z_{\mathrm{min}}, z_{\mathrm{max}}$ and free boundary conditions at $r = r_{\mathrm{max}}$ according to the method described by Malagón-Romero and Luque (2018). These free boundary conditions are consistent with the density charge inside the domain and with a potential decaying far away from the source. We have simulated positive and negative streamers propagating in background electric fields of 100 and 120 V/m, which correspond to 120 Td at 74.23 and 72.91 km, respectively. The simulated domain extends from 71 to 75 km in the vertical direction, and the grid resolution is 1 m. We have calculated the optical emissions from the streamer head in a moving cylindrical box of radius 150 m and height 150 m. We have also calculated the optical emissions from the glow in a cylindrical box of radius 30 m and height 700 m. Figure 1 shows a simulated positive streamer propagating downward for a background electric field of 100 V/m and a glow emerging at $z = 73.5$ km.

2.2. Laboratory Streamer

The ground-level streamer discharge develops in a needle-plane configuration. Our initial condition consists in a needle with an small ionization patch slightly off the needle tip. The needle is simulated by a narrow elongated volume with a high ionization. The initial electron density is thus the sum of a uniform background $n_e^{\mathrm{bg}} = 10^9 \mathrm{m}^{-3}$ plus

$$n_{\mathrm{e}}^{\mathrm{needle}} = n_{\mathrm{e0}} \exp\left(-\frac{\max\left(z - z_n, 0\right)^2}{\sigma_n^2} - \frac{r^2}{\sigma_n^2}\right), \tag{3}$$

and

$$n_e^{seed} = n_{e0} \exp\left(-\frac{(z - z_S)^2}{\sigma_S^2} - \frac{r^2}{\sigma_S^2}\right), \quad (4)$$

where $z_n = 5.4$ mm is the tip location, $z_S = 7.5$ mm is the center of the seed, and $\sigma_n = 0.9$ mm and $\sigma_S = 0.45$ mm are the e-folding radii and the electron density peaks at $n_{e0} = 10^{21}$ m^{-3}, respectively. The initial electron density is neutralized by an identical density of positive ions. Boundary conditions are the same as in the sprite streamer simulation. We have simulated positive and negative streamers with background electric fields $E_{bg} = \{12.5, 15, 20, 25\}$ kV/cm and $E_{bg} = \{15, 20, 25\}$ kV/cm, respectively. The full domain size is 3 cm × 1 cm, and the grid resolution is 5μm. We have calculated the optical emissions in a moving cylindrical box of radius 3.2 mm and a vertical extension between 0 and 3.2 mm containing the streamer head.

3. Spatial Nonuniformity of the Electric Field in Spectroscopic Diagnostics

In nonthermal air discharges, optical emissions are mainly determined by the concentration of electronically excited nitrogen molecules. The plasma involved in such electrical discharges is far from thermal equilibrium, ensuring that electron-impact processes driven by the electric field are responsible for the excitation of the emitting molecules. Radiative de-excitation processes, together with other chemical reactions, such as electronic quenching by air, contribute to the de-excitation of the excited molecules. The total number of emitted photons in nonequilibrium gas discharges depends on the reduced electric field and the competition between radiative de-excitation and other de-excitation processes.

In this section, we develop and compare two methods to estimate the peak electric field in a nonequilibrium plasma by considering the effect of the nonuniformity of the electric field. These methods pursue an estimation of the peak electric field from the ratio of optical emissions of different nitrogen band systems based on the spatial nonuniformity of the electric field (see Šimek, 2014 and references therein). In principle, these methods can be generalized to other gases than air if appropriate emission lines are identified.

3.1. Peak Electric Field From the Relation Between Electron and Electric Field Spatial Distributions

The density of the emitting species in a nonequilibrium plasma $N_s(t)$ can be estimated from the decay constant A' of the transitions that produce photons in a considered wavelength range and the observed intensity $I(t)$ as

$$N_s(t) = \frac{I(t)}{A'}. \quad (5)$$

The temporal production rate $S(t)$ due to electron impact can be derived from the continuity equation of the emitting species as

$$S(t) = \frac{dN_s(t)}{dt} + AN_s(t) + QN_s(t)N - CN'(t) + R(t), \quad (6)$$

where A is the total radiative decay constant of the emitting species and Q represents all the quenching rate constants by air molecules of density N. $N'(t)$ accounts for the density of all the upper species that populate the species by radiative cascade with radiative decay constants C. Finally, the term $R(t)$ includes the remaining loss processes, such as intersystem processes or vibrational redistribution. Obrusnik et al. (2018) and Bílek et al. (2018) demonstrated that the most important processes that influence the optical emissions are the excitation of emitting molecules by electron impact, radiative de-excitations, and electronic quenching. Therefore, we can neglect the effect of other processes in the derivation of the peak reduced electric field and approximate equation (6) as

$$S(t) \simeq \frac{dN_s(t)}{dt} + AN_s(t) + QN_s(t)N. \quad (7)$$

From equations (5) and (7), we can obtain the production ratios of two different species (1 and 2) at a fixed time t, given by $S_{12} = \frac{S_1}{S_2}$ as a first approximation, without considering any spatial nonuniformity of the electric field. The magnitude S_{12} and the electron-impact production ratio of species 1 and 2 given by $\nu_{12} = \frac{\nu_1(E/N)}{\nu_2(E/N)}$ allow us to estimate the reduced electric field that satisfies the equation

$$\frac{S_1}{S_2} \simeq \frac{\nu_1(E/N)}{\nu_2(E/N)}. \quad (8)$$

We get the values of $\nu_i(E/N)$ for all the considered species using BOLSIG+ for air (Hagelaar & Pitchford, 2005). This common approximation is useful to estimate the electric field value at the point where the rate of excitation is maximal (ε'). However, ε' is only equal to the peak electric field value in the discharge as long as the electric field is uniform. Optical emissions from nonthermal air discharges are generally produced by inhomogeneous electric fields, and streamers heads are a clear example (Celestin & Pasko, 2010; Naidis, 2009). Pérez-Invernón, Luquen, Gordillo-Vazquez, Sato, et al. (2018) investigated the spatial nonuniformity of the electric field and its effect on the optical emissions of halos and elves, two kinds of diffuse TLEs. They defined the function $H(\varepsilon)$ as the number of electrons under the influence of a reduced electric field (defined as $E_{\text{red}} = \frac{E}{N}$) larger than ε and weighted by the air density N:

$$H(\varepsilon) = \int d^3\mathbf{r}\, N(\mathbf{r})\, n_e(\mathbf{r})\, \theta\left(E_{\text{red}}(\mathbf{r}) - \varepsilon\right), \tag{9}$$

where $n_e(\mathbf{r})$ and $E_{\text{red}}(\mathbf{r})$ are, respectively, the electron density and the reduced electric field spatial distributions, and the integral extends over all the volume of the discharge. The symbol θ corresponds to the step function, being 1 if $E_{\text{red}} > \varepsilon$ or 0 in any other case. The total excitation rate of species i by electron impact in the spatial region occupied by the discharge can be written as a function of H as

$$\nu_i = \int_{E_{\text{red, min}}}^{E_{\text{red, max}}} d\varepsilon \left|\frac{dH}{d\varepsilon}\right| k_i(\varepsilon), \tag{10}$$

where $E_{\text{red, max}}$ and $E_{\text{red, min}}$ are, respectively, the maximum and the minimum reduced electric field in the region where the optical emissions are produced and $k_i(\varepsilon)$ is the reaction rate coefficient for electron-impact excitation of species i.

The function defined by equation (9) contains information about the spatial nonuniformity of the discharge. Pérez-Invernón, Luquen, Gordillo-Vazquez, Sato, et al. (2018) found that the function $H(\varepsilon)$ can be approximated as a linear function for halos and elves, as the electron density is not significantly affected by the electric field in those events. However, high values of the electric field in streamer heads produce an enhancement of some orders of magnitude in the background electron density. We have used the streamer model described in section 2 to find a general approximation to this function so we can use it in streamer and glow discharges. In particular, our approximation must fit the modeled curve in the electric field range where the maximum excitation of emitting molecules occurs. Examination of equation (10) indicates that the maximum excitation is produced at the electric field value where the product between the derivative $\frac{dH}{d\varepsilon}$ and the electron-impact excitation rate coefficient reaches its maximum. Then, the spatial nonuniformity of the electric field can influence the value of the electric field that produces the maximum excitation.

Solid black lines in Figure 2 show the normalized function H (equation 9) obtained for two streamer heads simulated at different pressures and for a low pressure streamer glow. Dashed black lines in Figure 2 correspond to the normalized derivative $\frac{dH}{d\varepsilon}$. Finally, color solid lines in Figure 2 show the normalized product between $\frac{dH}{d\varepsilon}$ and different electron-impact excitation rate coefficients. The approximation to H must fit the solid black lines in Figure 2 in the electric field range where the product between $\frac{dH}{d\varepsilon}$ and the electron-impact excitation rate coefficient is greater than zero. It can be clearly seen in Figure 2 that most emissions produced in the glow are located in the region where the electric field reaches its maximum value. Therefore, the method neglecting the spatial nonuniformity to estimate the peak electric field is accurate enough to study glows. However, the situation is different in streamer heads, where the maximum excitation is not produced in the region where the electric field reaches its maximum. Therefore, we need to develop a method accounting for the spatial nonuniformity of the electric field distribution.

By definition, the function H is constant between 0 Td and the minimum field that influences electrons, $E_{\text{red, min}}$. Figure 2 shows that for streamer heads, H decreases between $E_{\text{red, min}}$ and $E_{\text{red, max}}$, while $H(E_{\text{red, max}}) = 0$ by definition. Regarding halos and elves (Pérez-Invernón, Luquen, Gordillo-Vazquez, Sato, et al., 2018), H could be approximated as a linear function. However, a higher order approximation is convenient in the case of streamer heads. We have examined the electric field dependence of H, concluding that it can be approximated in general as

$$H(\varepsilon) \simeq \alpha\left(E_{\text{red, max}} - \varepsilon\right)^{\beta}, \tag{11}$$

where α and β are constants.

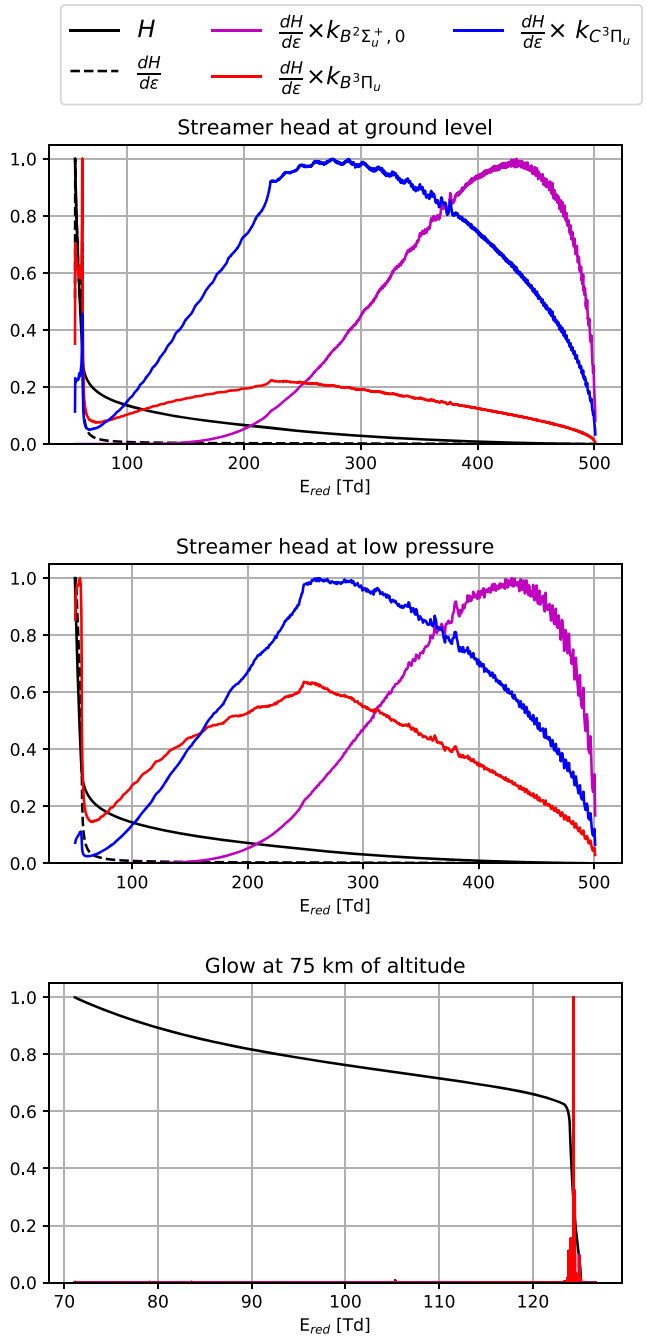

Figure 2. Function H (black solid lines), $\frac{dH}{d\varepsilon}$ (dashed black lines), and product between $\frac{dH}{d\varepsilon}$ and the electron-impact reaction rate coefficient k_i indicating the electric field range where excitation of emitting molecules is important (color solid lines). We plot the results for a positive streamer at atmospheric pressure with a background electric field of 20 kV/cm and 65 ns after its onset (first panel), a positive streamer at low pressure with a background electric field of 100 V/m and 0.9 ms after its onset (second panel), and its glow 0.9 ms after its onset (third panel). All curves are normalized to their maximum value.

We have performed seven negative and positive laboratory-like streamer simulations with different background electric fields (12.5, ±15, ±20, and ±25 kV/cm) and four negative and positive sprite-like streamer simulations (71 to 75 km) with different background electric fields (±100 and ±120 V/m). The value of the obtained functions H ranges between zero and several orders of magnitude in all cases. Therefore, we have used a logarithmic least square fitting of equation (11) in order to minimize the error of the coefficients α and β. The fitting of equation (11) has been performed in an equispaced grid of electric field values to ensure

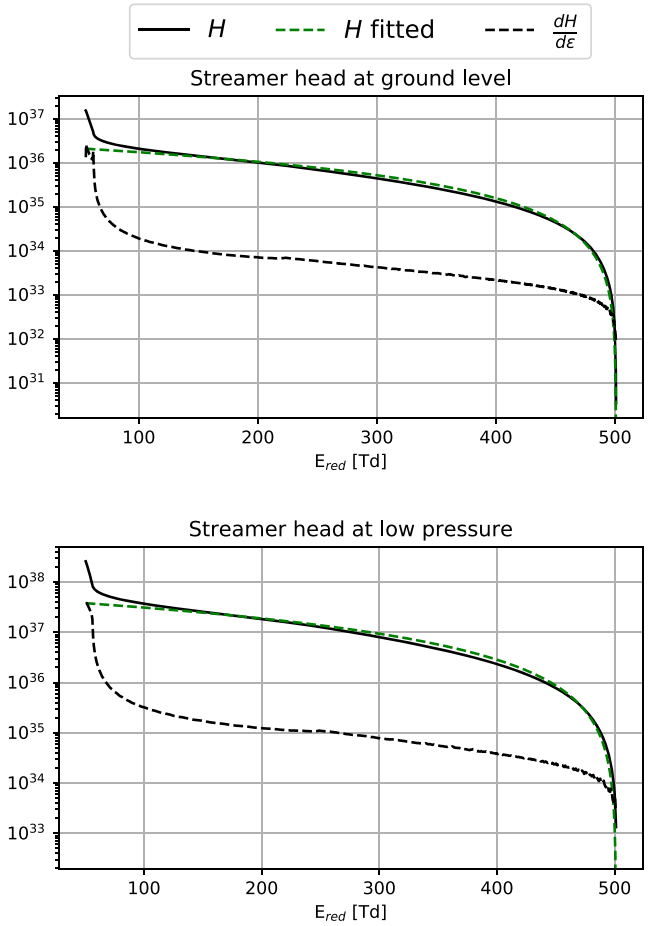

Figure 3. Reduced electric field dependence of the function H (black solid lines) and the fitting of H using equation (11) (dashed green lines) and $\frac{dH}{d\varepsilon}$ (dashed black lines). We plot the results for a positive streamer at atmospheric pressure with a background electric field of 20 kV/cm and 65 ns after its onset (first panel) and for a positive streamer at low pressure with a background electric field of 100 V/m and 0.9 ms after its onset (second panel).

that the minimization of the error weighting does not depend on the distribution of points of the functions H calculated by the streamer model. We plot the function H together with the obtained fitting and the derivative $\frac{dH}{d\varepsilon}$ for laboratory and sprite streamer heads in Figure 3. We have obtained that the β exponent is between 1.8 and 2.0 with a mean squared error of about 6×10^{-3} for all the laboratory streamers and between 1.95 and 2.09 with a mean squared error of about 10^{-2} for all the sprite streamers. Thus, these values do not significantly depend on the streamer polarity, background electric field, or pressure. Consequently, we take the average value $\beta = 1.96$. As the β exponent is always close to 2, we will refer to this diagnostic method as "quadratic method." The obtained values of α are about 5×10^{31} with a mean squared error of about 1.5×10^{30} for laboratory streamers and about 10^{33} with a mean squared error of about 5×10^{31} for sprite streamers.

Let us now deduce the expression for the production of emitting species by electron impact considering this approximation to H. Applying the derivative to equation (11), equation (10) can be written as

$$\nu_i = \beta\,\alpha \int_{E_{\text{red, min}}}^{E_{\text{red, max}}} d\varepsilon \left(E_{\text{red, max}} - \varepsilon\right)^{\beta-1} k_i(\varepsilon). \tag{12}$$

Now, following equations (8) and (12), we write the production rate ratio of two species by electron impact derived from the recorded optical intensity $\left(S_{12} = \frac{S_1}{S_2}\right)$ as

$$S_{12} = \frac{S_1}{S_2} \simeq \frac{\int_{E_{\text{red, min}}}^{E_{\text{red, max}}} d\varepsilon \left(E_{\text{red, max}} - \varepsilon\right)^{\beta-1} k_1(\varepsilon)}{\int_{E_{\text{red, min}}}^{E_{\text{red, max}}} d\varepsilon \left(E_{\text{red, max}} - \varepsilon\right)^{\beta-1} k_2(\varepsilon)}. \tag{13}$$

In order to derive $E_{\text{red,max}}$, we need to know the minimum electric field in the region where the optical emissions are produced. In general, $E_{\text{red,min}}$ is reached in the region just behind the streamer head, and this is lower than the background electric field. We can estimate how the choice $E_{\text{red, min}} = 0$ affects the results by writing equation (13) as

$$S_{12} \simeq \frac{P_1(1-\gamma_1)}{P_2(1-\gamma_2)}, \tag{14}$$

where we define

$$P_i = \int_0^{E_{\text{red, max}}} d\varepsilon \left(E_{\text{red, max}} - \varepsilon\right)^{\beta-1} k_i(\varepsilon), \tag{15}$$

and

$$\gamma_i = \frac{\int_0^{E_{\text{red, min}}} d\varepsilon \left(E_{\text{red, max}} - \varepsilon\right)^{\beta-1} k_i(\varepsilon)}{P_i}, \tag{16}$$

and calculating the value of the ratio of $(1-\gamma_1)$ to $(1-\gamma_2)$ using the streamer model at two different pressures, polarities, and background electric fields. The value of this ratio ranges from 2.6 (negative laboratory streamer at atmospheric pressure with a background electric field of −15 kV/cm) to 2.9 (positive sprite streamer with a background electric field of −120 V/m). Therefore, the assumption that $E_{\text{red, min}} = 0$ in equation (13) for the diagnostic of streamer heads can introduce an error in the estimated production ratio of a factor 3 according to equation (14). This error results in an uncertainty of a 25% over the estimated peak electric field.

3.2. Peak Electric Field Under the Assumption of Planar Geometry

Lagarkov and Rutkevich (1994, p. 62) derived a relation between the electric field and the ionization level in a flat ionization front. Li et al. (2007) employed this relation to calculate the ionization of air molecules in

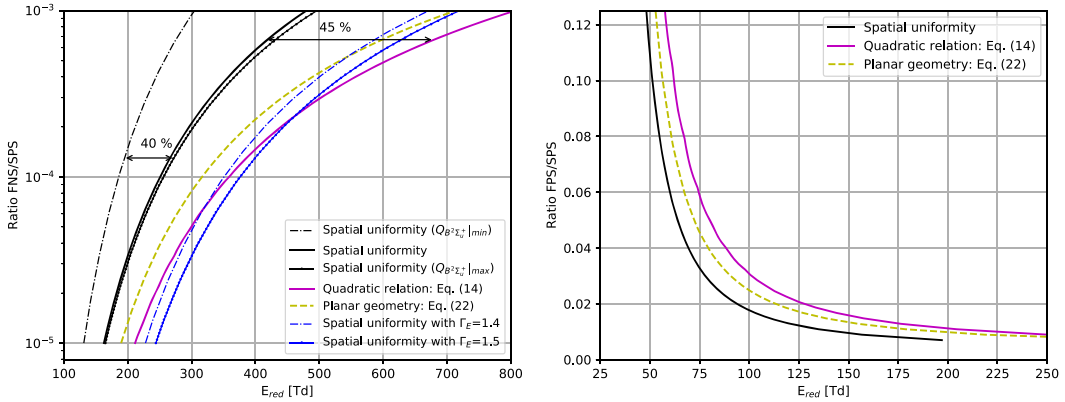

Figure 4. Reduced electric field dependence of the ratios $FNS_{(0,v'')}$/SPS (left panel) and FPS/SPS (right panel) at atmospheric pressure assuming (1) spatial uniformity of the electric field distribution according to equation (8) (black solid line), (2) spatial nonuniformity of the electric field distribution according to equation (13) (purple solid line), (3) planar geometry of the electric field according to equation (21) (yellow dashed line), and (4) spatial uniformity of the electric field distribution with Γ_E=1.4 and Γ_E=1.5 (Celestin & Pasko, 2010; blue lines). The employed reaction rate coefficients are collected in Table 1.

streamer heads. Li et al. (2007) and Dubrovin et al. (2014) derived a relation between the electric field and the ionization level in a planar ionization front. In this section, we extend the results of Li et al. (2007) and Dubrovin et al. (2014) to show that there is also a relation between the molecular excitation level and the electric field. The resulting relation can be used to estimate the peak electric field in ionization fronts.

The characteristic time of dielectric screening in a nonequilibrium plasma can be written as

$$\tau_d = \frac{\epsilon_0}{\sigma}, \tag{17}$$

where ϵ_0 is the vacuum permittivity and σ stands for the electrical conductivity, which we assume is dominated by electrons. This conductivity is determined by the product of the elementary charge (e), the electron mobility (μ_e), and the electron density (n_e).

Assuming a planar geometry and an external electric field that varies slowly (Li et al., 2007; Dubrovin et al., 2014), the local electric field (ε) evolves as

$$\frac{d\varepsilon}{dt} = -\frac{e\mu_e n_e}{\epsilon_0}\varepsilon = -\frac{\varepsilon}{\tau_d}. \tag{18}$$

In a nonequilibrium plasma, the production rate of electronically excited molecules N_i by electron impact is given by

$$\nu_i = \frac{dN_i}{dt} = Nk_i(\varepsilon)n_e, \tag{19}$$

where $k_i(\varepsilon)$ is the reaction rate coefficient and we have neglected other processes that affect N_i.

The relation between the density of excited molecules and the electric field (Lagarkov & Rutkevich, 1994) can be obtained from equations (18) and (19),

$$N_i = \int_{E_{\mathrm{red,\,min}}}^{E_{\mathrm{red,\,max}}} d\varepsilon \frac{N\epsilon_0}{e\mu_e}\frac{k_i(\varepsilon)}{\varepsilon}. \tag{20}$$

On the other hand, the ratio between the density of two electronically excited molecules ($N_{12} = N_1/N_2$) deduced from the recorded optical intensity and assuming that the electron mobility is not electric field dependent can be written as

$$N_{12} \simeq \frac{\int_{E_{\mathrm{red,\,min}}}^{E_{\mathrm{red,\,max}}} \varepsilon^{-1}k_1(\varepsilon)d\varepsilon}{\int_{E_{\mathrm{red,\,min}}}^{E_{\mathrm{red,\,max}}} \varepsilon^{-1}k_2(\varepsilon)d\varepsilon}. \tag{21}$$

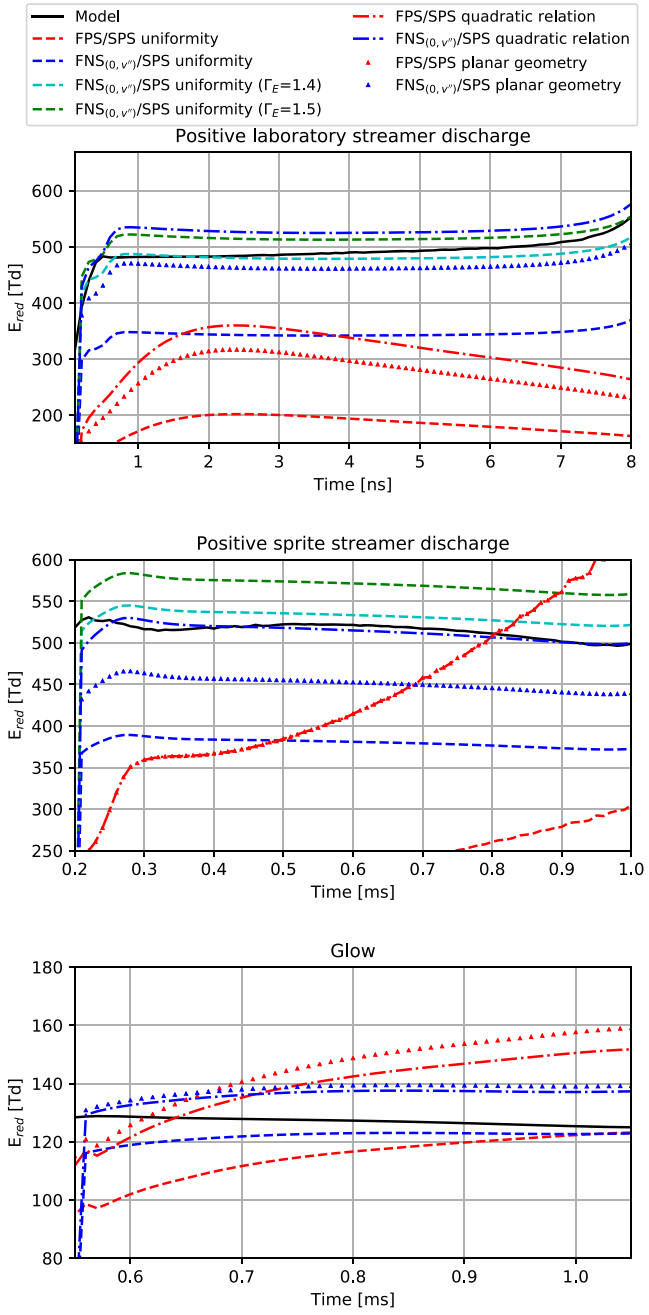

Figure 5. Temporal evolution of the electric field peak in the head of two computationally simulated streamers at different pressures and in a glow discharge. Lines are as follows: Peak electric field given by the model (black solid color lines), deduced peak electric field considering that the electric field is homogeneously distributed in space (dashed color lines), deduced peak electric field considering nonuniformity of the electric field (dashed doted color lines), and deduced peak electric field considering planar geometry of the electric field (triangle color lines). The nonplotted peak electric fields obtained by the ratio of $FNS_{(1,v'')}$ to SPS are similar to the plotted peak electric fields obtained by the ratio of $FNS_{(0,v'')}$ to SPS.

Equation (21) is an alternative to equation (13). Equation (21) does not depend on any particular parameter. However, using equation (21) to derive the peak electric field in the discharge also requires knowing the minimum electric field in the region where the optical emissions are produced. We can use equations (14), (15), and (16) together with equation (21) to evaluate the uncertainty in the estimated peak electric field under the assumption $E_{\text{red, min}} = 0$. The value of the ratio $(1-\gamma_1)$ to $(1-\gamma_2)$ ranges between $1+3\times10^{-5}$ (positive laboratory streamer with a background electric field of −12.5 kV/cm) and $1+7\times10^{-4}$ (positive sprite streamer with a background electric field of 120 V/m). Hence, the assumption $E_{\text{red, min}} = 0$ in equation (21) does not introduce a significant error in this diagnostic method. In the same manner, a possible estimation of the minimum electric field in the streamer channel does not improve this method.

4. Comparison of Methods and Discussion

In this section, we compare the two methods described in sections 3.2 and 3.1. Following the notation by Celestin and Pasko (2010), we define Γ_E as the ratio between the peak electric field in the streamer simulation and the peak electric field derived from optical diagnostic methods.

Let us first investigate the dependence between the peak electric field and the considered emission ratios. In Figure 4, we plot the peak electric field dependence of the emission ratios $FNS_{(0,v'')}$/SPS and FPS/SPS using the described methods and the reaction rate coefficients of Table 1. We have also calculated the peak electric field dependence of the emission ratio $FNS_{(0,v'')}$/SPS using the lowest and highest quenching rates of $N_2^+(B^2\Sigma_u^+)$ by air provided by Bílek et al. (2018). Comparison between the averaged uncertainty due to the quenching rates (40%) and the spatial nonuniformity (45%) in Figure 4 shows that the effect of the spatial nonuniformity of the discharge in the estimation of the peak electric field from the $FNS_{(0,v'')}$ to SPS ratio is of the same order to that of quenching. The right panel of Figure 4 indicates that the ratio FPS/SPS cannot provide accurate information about the peak electric field above ~200 Td.

Figure 5 shows the result of applying the peak electric field estimation methods to a streamer head simulated at atmospheric pressure, a streamer head at low pressure (71 to 75 km), and a glow segment inside a streamer channel at low pressure. Dashed lines correspond to the peak electric field considering that the electric field is homogeneously distributed in space. Dotted and dashed dotted color lines are the electric field peak considering that the electric field is inhomogeneously distributed in space.

Considering that the electric field is inhomogeneously distributed in space in streamer heads is clearly justified. The "quadratic relation method" and the "planar geometry method" improve the estimation of the peak electric field with respect to the "uniformity method" for streamer discharges. In addition, the "quadratic relation method" improves the estimation of the peak electric field with respect to the "uniformity method" using correction factor for the positive sprite streamer discharge.

However, doing the same to study the glow introduces more error than assuming an electric field homogeneously distributed. Figure 5 also shows that the ratio of FPS to SPS does not provide enough information about the electric field in the streamer head, where the electric field is above 200 Td.

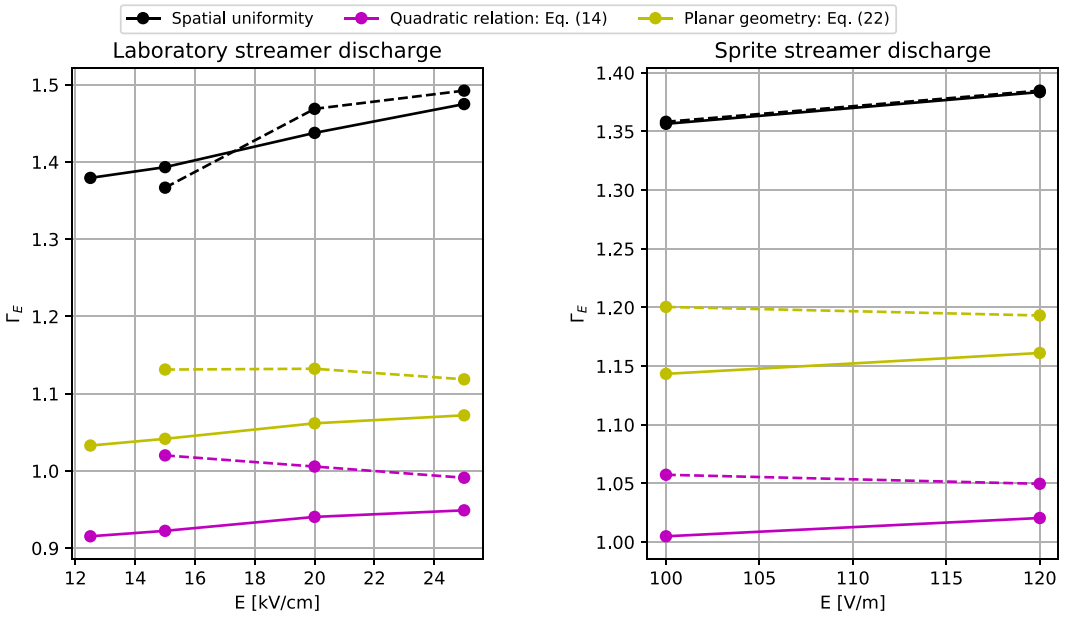

Figure 6. Ratio Γ_E between the peak electric field in the streamer simulation and the peak electric field estimated using different diagnostic methods and the emissions coefficient $FNS_{(0,v'')}$/SPS. Dashed and solid lines correspond to negative and positive streamers, respectively. Please note that in the sprite case (right plot), 100 V/m corresponds to 120 Td at 74.23 km and 120 V/m corresponds to 120 Td at 72.91 km.

In Figure 6, we plot the time-averaged Γ_E coefficient for the considered diagnostic methods in streamer heads. Γ_E ranges between ~1.4 and 1.5 and increases with the background electric field for the method based on the uniformity of the electric field, as previously reported by Celestin and Pasko (2010). On the other hand, Γ_E ranges between ~0.9 and 1.2 and has a weaker dependence on the background electric field for the methods that introduce the nonuniformity of the electric field.

Following Paris et al. (2005), we derive empirical formulae for the relationship between the intensity ratio FNS/SPS in streamer discharges and the peak reduced electric field using the quadratic diagnostic method based on the relationship between the electron and the electric field spatial distributions:

$$R_{\mathrm{FNS/SPS}} = \exp\left[a\left(-b\left(E_{\mathrm{red}}\right)^{c} - d\left(E_{\mathrm{red}}\right)^{e}\right)\right], \tag{21}$$

where the coefficients a, b, c, d, and e are provided for different streamers discharges and emissions lines in Table 2. The electric field dependence of $R_{391.4/337}$, $R_{391.4/399.8}$, $R_{427.8/337}$, and $R_{427.8/337}$ are calculated taking the quenching rate constants, the radiative decay constants, and the cross sections of electronic excitation of $N_2(C^3\Pi_u, v = 0)$ and $N_2(C^3\Pi_u, v = 1)$ from Gordillo-Vázquez (2010) and Pérez-Invernón, Luque, & Gordillo-Vázquez (2018). The employed quenching rate constants, radiative decay constants, and cross-sections of electronic ionization and excitation of $N_2^+(B^2\Sigma_u^+, v = 0)$ and $N_2^+(B^2\Sigma_u^+, v = 1)$ are listed in Table 1.

Table 2
Coefficients a, b, c, d, and e of Equation (21) for Different Streamer Discharges and Emissions Lines

Type of streamer	Ratio of lines	a, b, c, d, e
Laboratory streamer	$R_{391.4/337}$	2.22×10^{2}, 0.41, −0.39, 3.93×10^{2}, −1.89
	$R_{427.8/337}$	32.88, 60.24, −0.98, 0.15, -4.10×10^{-4}
	$R_{427.8/399.8}$	1.93×10^{3}, 3.86×10^{3}, −2.82, 7.89×10^{-2}, −0.46
	$R_{391.4/399.8}$	1.67×10^{2}, 0.15, −0.24, 46.44, −1.31
Sprite streamer	$R_{391.4/337}$	1.01×10^{5}, 9.74×10^{-3}, −0.84, 2.02×10^{5}, −4.59
	$R_{427.8/337}$	1.54×10^{5}, 3.08×10^{5}, −4.63, 3.92×10^{-3}, −0.74
	$R_{427.8/399.8}$	3.45×10^{3}, 6.90×10^{3}, −3.16, 0.52, −0.72
	$R_{391.4/399.8}$	82.37, 9.97×10^{7}, -4.08×10^{5}, 1.68, −0.90

5. Application of the Described Methods to Experimental Data

Armstrong et al. (1998) reported the ratio of $SPS_{(1,4)}$ (399.8 nm) to $FNS_{(1,0)}$ (427.8 nm) emitted by TLEs detected from the FMA Research Yucca Ridge Field station, located at an altitude of about 1,500 m. The photometric measurements in the SPRITE's 1995 and 1996 campaigns reported by Armstrong et al. (1998) were recorded using two photometers with a time resolution of 1.3 ms. Armstrong et al. (1998) discussed the overlap between the SPS and the FNS bands in the 427.8-nm photometer due to the wavelength dependence of the response of the employed instruments. According to their estimation, the signal of the SPS in the 427.8-nm photometer corresponds to approximately 26% of the signal in the 399.8-nm photometer. Therefore, 26% of the signal reported by the 399.8-nm photometer has to be subtracted from the signal recorded by the 427.8-nm photometer to get the true contribution of the FNS.

In this section, we estimate the peak electric field using the reported intensity ratio of two sprites referred as "DAY 201 - 19050651" and "DAY 201 - 19062205" in Armstrong et al. (1998). The field of view of the photometers covers a large spatial region of the sprites (see in Figures 5 and 6 of Armstrong et al., 1998). Thus, the reported intensity ratio is a combination of the optical emissions of the streamers and glows that form the sprite. Unfortunately, we cannot separate optical emissions from streamers and glows to decide the convenience of considering that the electric field is homogeneously or inhomogeneously distributed in space. Then, we calculate the peak electric field from the reported ratio using both methods. We follow the same procedure:

1. The reported ratios of $SPS_{(1,4)}$ (399.8 nm) to $FNS_{(1,0)}$ (427.8 nm) for the sprites "DAY 201 - 19050651" and "DAY 201 - 19062205" in Armstrong et al. (1998) are, respectively, 1.91 and 2.84 when the maximum luminosity is reached. We correct these ratios by considering that the signal of the SPS in the 427.8-nm photometer corresponds to approximately 26% of the signal in the 399.8-nm photometer (Armstrong et al., 1998).
2. The observed ratio of intensities is influenced by the atmospheric transmittance. The sprites were triggered by a storm, which was located ~260 km away from the observer (Armstrong et al., 1998), while the observatory station altitude is ~1,500 m above sea level. In addition, we assume that the optical emissions are produced at ~70 km, which is a characteristic altitude of sprites (Luque et al., 2016; Stenbaek-Nielsen et al., 2010). Therefore we can calculate the optical transmittance of the atmosphere between the sprites and the photometers using the software MODTRANS 5 (Berk et al., 2005). We use the calculated optical transmittance to obtain the emitted ratio of intensities from the recorded signal.
3. We calculate the production of emitting molecules by electron impact using equations (5) and (6) and assuming the air density at an altitude of 70 km. We use the reaction rate coefficients of Table 1 to calculate the density of $N_2^+(B^2\Sigma_u^+, v = 1)$. The vibrational kinetics employed to calculate the density of $N_2(C^3\Pi_u, v' = 1)$ is taken from Gordillo-Vázquez (2010) and Pérez-Invernón, Luque, & Gordillo-Vázquez (2018).
4. We estimate the peak electric field in the sprites by considering a homogeneously (inhomogeneously) distributed electric field in space according to equation (8) (equations 13 or 21) with $E_{\text{red, min}}$ equal to zero.

The resulting peak electric field for the sprite "DAY 201 - 19050651," if we assume a homogeneously distributed electric field in space, is 450 Td, while for the sprite "DAY 201 - 19062205," the peak electric field is 326 Td. Using the previously defined quadratic method (equations 13), the resulting peak electric field for the sprite "DAY 201 - 19050651" is 757 Td, while for the sprite "DAY 201 - 19062205," the peak electric field is 503 Td. The use of equation (21) would lead to slightly lower reduced electric fields, as seen in Figure 4. As photometers cannot spatially resolve the emissions, we are probably analyzing combined optical emissions from streamer heads and glows. Therefore, we cannot determine which method is the most accurate in this case. As the reported intensities are a combination of the intensities emitted by streamers and glows, we can assume that the value of the peak electric fields in streamer heads of the sprites "DAY 201 - 19050651" and "DAY 201 - 19062205" are respectively in the range 451–757 Td and 327–503 Td. These derived values are probably influenced by the peak electric field inside glows (on the order of 120 Td; Luque et al., 2016) and streamer heads (several hundreds of Townsends). We have repeated these calculations for the case of a sprite altitude of 80 km instead of 70 km, obtaining an increase in the peak electric fields of 1.5%.

6. Conclusions

We have used a streamer model to simulate streamer heads and glows to quantify the influence of the nonuniformity of the electric field in spectroscopic diagnostic methods. The analysis of the spatial inhomogeneity of the electric field in air discharges has allowed us to improve the optical diagnostic methods commonly employed in the determination of the peak electric field in streamer heads. The commonly employed method underestimates the peak electric field by about 40–50%, while the methods developed in this work reduce the uncertainty to about 10–20%. We have also shown that the ratio of FPS to SPS can be employed to deduce the peak electric field in streamer glows without considering the spatial inhomogeneity of the electric field.

The first developed optical diagnostic method (section 3.1) is based on the characterization of the nonuniformity of the electric field in streamer heads using a streamer model. This method introduces an exponent ($\beta \simeq 2$) that is almost constant for different streamer configurations. The most important uncertainty in the peak electric field calculated with this method is due to the uncertainty in the electric field inside the streamer channel. In general, the value of $E_{\mathrm{red,\,min}}$ is unknown. Hence, we propose to set $E_{\mathrm{red,\,min}} = 0$.

The second developed optical diagnostic method (section 3.2) is based on the relation between the electric field and the level of molecular excitation in a planar ionization front. This method does not introduce any extra parameter to estimate the peak electric field, and considering $E_{\mathrm{red,\,min}} = 0$ does not introduce a significant error. Thus, in general, it is more convenient than the method described in section 3.1. However, the method described in section 3.1 can be useful whenever the estimation of the electric field in the streamer channel is possible. In principle, both methods can be generalized to other gases if the appropriate emission lines are identified.

Despite the improvements, optical diagnostic methods of air discharges from the ratio of FNS to SPS at atmospheric pressure are still very sensitive to the considered chemical reactions rates (Obrusnik et al., 2018; Bílek et al., 2018). As Obrusnik et al. (2018) and Bílek et al. (2018) concluded, more efforts are needed for a more precise determination of the reaction rates (especially quenching rates) that are important for diagnostic methods based on the FNS emission at atmospheric pressure.

The uncertainty in the reaction rates employed in the determination of the peak electric field from the ratio of FPS to SPS is lower than the uncertainty in the reaction rates involved in the FNS emissions. Nevertheless, the FPS/SPS ratio of intensities is only applicable for glow discharges where the electric field is known to be below ~200 Td.

Acknowledgments
This work was supported by the Spanish Ministry of Science and Innovation, MINECO under project ESP2017-86263-C4-4-R and by the EU through the European Research Council (ERC) under the European Union's H2020 programm/ERC grant agreement 681257. This project has received funding from the European Union's Horizon 2020 research and innovation programme under the Marie Skłodowska-Curie grant agreement SAINT 722337. The authors acknowledge financial support from the State Agency for Research of the Spanish MCIU through the "Center of Excellence Severo Ochoa" award for the Instituto de Astrofísica de Andalucía (SEV-2017-0709). F. J. P. I. acknowledges a PhD research contract, code BES-2014-069567. Data and codes used to generate figures presented here are available at https://cloud.iaa.csic.es/public.php?service=files&t=54fcc1134f55efa61087670678226236.

References

Adachi, T., Fukunishi, H., Takahashi, Y., Hiraki, Y., Hsu, R.-R., Su, H.-T., et al. (2006). Electric field transition between the diffuse and streamer regions of sprites estimated from ISUAL/array photometer measurements. *Geophysical Research Letters*, *33*, L17803. https://doi.org/10.1029/2006GL026495

Alghamdi, A., Ahmadia, A., Ketcheson, D. I., Knepley, M. G., Mandli, K. T., & Dalcin, L. (2011). Petclaw: A scalable parallel nonlinear wave propagation solver for python. In *Proceedings of the 19th High Performance Computing Symposia, HPC '11*, Society for Computer Simulation International, San Diego, CA, USA, pp. 96–103.

Armstrong, R. A., Shorter, J. A., Taylor, M. J., Suszcynsky, D. M., Lyons, W. A., & Jeong, L. S. (1998). Photometric measurements in the SPRITES 1995 and 1996 campaigns of nitrogen second positive (399.8 nm) and first negative (427.8 nm) emissions. *Journal of Atmospheric and Solar-Terrestrial Physics*, *60*, 787. https://doi.org/10.1016/S1364-6826(98)00026-1

Balay, S. (2016). PETSc users manual (*ANL-95/11 - Revision 3.7*): Argonne National Laboratory.

Balay, S., Abhyankar, S., Adams, M. F., Brown, J., Brune, P., Buschelman, K., & Zhang, H. (2016). PETSc Web page. Retrieved from http://www.mcs.anl.gov/petsc

Berk, A., Anderson, G. P., Acharya, P. K., Bernstein, L. S., Muratov, L., Lee, J., et al. (2005). MODTRAN 5: A reformulated atmospheric band model with auxiliary species and practical multiple scattering options: Update, *Algorithms and technologies for multispectral, hyperspectral, and ultraspectral imagery XI* (Vol. 5806, pp. 662–668): International Society for Optics and Photonics.

Bílek, P., Obrusnik, A., Hoder, T., Šimek, M., & Bonaventura, Z. (2018). Electric field determination in air plasmas from intensity ratio of nitrogen spectral bands: II. Reduction of the uncertainty and state-of-the-art model. *Plasma Sources Science and Technology*, *27*, 085012. https://doi.org/10.1088/1361-6595/aad666

Bonaventura, Z., Bourdon, A., Celestin, S., & Pasko, V. P. (2011). Electric field determination in streamer discharges in air at atmospheric pressure. *Plasma Sources Science and Technology*, *20*(3), 035012. https://doi.org/10.1088/0963-0252/20/3/035012

Bruggeman, P. J., Iza, F., & Brandenburg, R. (2017). Foundations of atmospheric pressure non-equilibrium plasmas. *Plasma Sources Science and Technology*, *26*(12), 123002.

Capitelli, M., Ferreira, C. M., Gordiets, B. F., & Osipov, A. I. (2000). *Plasma kinetics in atmospheric gases*. Berlin, Germany: Springer Verlag.

Celestin, S., & Pasko, V. P. (2010). Effects of spatial non-uniformity of streamer discharges on spectroscopic diagnostics of peak electric fields in transient luminous events. *Geophysical Research Letters*, *37*, L07804. https://doi.org/10.1029/2010GL042675

Clawpack Development Team (2017). Clawpack software. https://doi.org/10.5281/zenodo.820730, version 5.4.1.

Creyghton, Y. (1994). *Pulsed positive corona discharges: Fundamental study and application to flue gas treatment*: Technische Universiteit Eindhoven.

Dilecce, G., Ambrico, P. F., & De Benedictis, S. (2010). On the collision quenching of $N_2^+(B^2\Sigma_u^+, v=0)$ by N_2 and O_2 and its influence on the measurement of E/N by intensity ratio of nitrogen spectral bands. *Journal of Physics D*, *43*(19), 195201. https://doi.org/10.1088/0022-3727/43/19/195201

Dubrovin, D., Luque, A., Gordillo-Vázquez, F. J., Yair, Y., Parra-Rojas, F. C., Ebert, U., & Price, C. (2014). Impact of lightning on the lower ionosphere of Saturn and possible generation of halos and sprites. *Icarus*, *241*, 313. https://doi.org/10.1016/j.icarus.2014.06.025

Franz, R. C., Nemzek, R. J., & Winckler, J. R. (1990). Television image of a large upward electrical discharge above a thunderstorm system. *Science*, *249*, 48. https://doi.org/10.1126/science.249.4964.48

Gallimberti, I., Hepworth, J. K., & Klewe, R. C. (1974). Spectroscopic investigation of impulse corona discharges. *Journal of Physics D*, *7*, 880. https://doi.org/10.1088/0022-3727/7/6/315

Gilmore, F. R., Laher, R. R., & Espy, P. J. (1992). Franck-Condon factors, r-centroids, electronic transition moments, and Einstein coefficients for many nitrogen and oxygen band systems. *Journal of Physical and Chemical Reference Data*, *21*, 1005. https://doi.org/10.1063/1.555910

Goldman, M., & Goldman, A. (1978). Chapter 4 - Corona discharges. In M. N. Hirsh, & H. J. Oskam (Eds.), *Gaseous electronics*, Electrical discharges (Vol. 1, pp. 219–290). Minneapolis, MN: Academic Press. https://doi.org/10.1016/B978-0-12-349701-7.50009-2

Gordillo-Vázquez, F. J. (2010). Vibrational kinetics of air plasmas induced by sprites. *Journal of Geophysical Research*, *115*, A00E25. https://doi.org/10.1029/2009JA014688

Gordillo-Vázquez, F. J., & Donkó, Z. (2009). Electron energy distribution functions and transport coefficients relevant for air plasmas in the troposphere: Impact of humidity and gas temperature. *Plasma Sources Science and Technology*, *18*(3), 34021. https://doi.org/10.1088/0963-0252/18/3/034021

Gordillo-Vázquez, F. J., & Luque, A. (2010). Electrical conductivity in sprite streamer channels. *Geophysical Research Letters*, *37*, L16809. https://doi.org/10.1029/2010GL044349

Gordillo-Vázquez, F. J., Passas, M., Luque, A., Sánchez, J., Velde, O. A., & Montanyá, J. (2018). High spectral resolution spectroscopy of sprites: A natural probe of the mesosphere. *Journal of Geophysical Research: Atmospheres*, *123*, 2336–2346. https://doi.org/10.1002/2017JD028126

Hagelaar, G. J. M., & Pitchford, L. C. (2005). Solving the Boltzmann equation to obtain electron transport coefficients and rate coefficients for fluid models. *Plasma Sources Science and Technology*, *14*, 722. https://doi.org/10.1088/0963-0252/14/4/011

Hoder, T., Simek, M., Bonaventura, Z., Prukner, V., & Gordillo-Vázquez, F. J. (2016). Radially and temporally resolved electric field of positive streamers in air and modelling of the induced plasma chemistry. *Plasma Sources Science and Technology*, *25*, 45021. https://doi.org/10.1088/0963-0252/25/4/045021

Hoder, T., Černák, M., Paillol, J., Loffhagen, D., & Brandenburg, R. (2012). High-resolution measurements of the electric field at the streamer arrival to the cathode: A unification of the streamer-initiated gas-breakdown mechanism. *Physical Review E*, *86*(5), 55401.

Ihaddadene, M. A., & Celestin, S. (2017). Determination of sprite streamers altitude based on N_2 spectroscopic analysis. *Journal of Geophysical Research: Space Physics*, *122*, 1000–1014. https://doi.org/10.1002/2016JA023111

Jolly, J., & Plain, A. (1983). Determination of the quenching rates of N_2^+ ($B^2\Sigma_u^+$, $v=0$, 1) by n2 using laser-induced fluorescence. *Chemical physics letters*, *100*(5), 425–428.

Kim, Y., Hong, S. H., Cha, M. S., Song, Y.-H., & Kim, S. J. (2003). Measurements of electron energy by emission spectroscopy in pulsed corona and dielectric barrier discharges. *Journal of Advanced Oxidation Technologies*, *6*(1), 17–22.

Kondo, K., & Ikuta, N. (1980). Highly resolved observation of the primary wave emission in atmospheric positive-streamer corona. *Journal of Physics D: Applied Physics*, *13*(2), L33.

Kozlov, K., Wagner, H., Brandenburg, R., & Michel, P. (2001). Spatio-temporally resolved spectroscopic diagnostics of the barrier discharge in air at atmospheric pressure. *Journal of Physics D: Applied Physics*, *34*(21), 3164.

Kuo, C.-L., Chou, J. K., Tsai, L. Y., Chen, A. B., Su, H. T., Hsu, R. R., et al. (2009). Discharge processes, electric field, and electron energy in ISUAL-recorded gigantic jets. *Journal of Geophysical Research*, *114*, A04314. https://doi.org/10.1029/2008JA013791

Kuo, C.-L., Hsu, R., Chen, A., Su, H., Lee, L.-C., Mende, S., et al. (2005). Electric fields and electron energies inferred from the ISUAL recorded sprites. *Geophysical research letters*, *32*, L19103. https://doi.org/10.1029/2005GL023389

Kuo, C. L., Su, H. T., & Hsu, R. R. (2015). The blue luminous events observed by ISUAL payload on board FORMOSAT-2 satellite. *Journal of Geophysical Research: Space Physics*, *120*, 9795–9804. https://doi.org/10.1002/2015JA021386

Kuo, C.-L., Williams, E., Bór, J., Lin, Y. H., Lee, L. J., Huang, S. M., et al. (2013). Ionization emissions associated with N_2^+ 1N band in halos without visible sprite streamers. *Journal of Geophysical Research: Space Physics*, *118*, 5317–5326. https://doi.org/10.1002/jgra.50470

Lagarkov, A. N., & Rutkevich, I. M. (1994). *Ionization waves in electrical breakdown of gases*. 175 Fifth Avenue, New York, NY 10010, USA: Springer-Verlag New York, Inc.

LeVeque, R. (2002). *Finite volume methods for hyperbolic problems*. Cambridge University Press: Cambridge Texts in Applied Mathematics.

Li, C., Brok, W. J. M., Ebert, U., & van der Mullen, J. J. A. M. (2007). Deviations from the local field approximation in negative streamer heads. *Journal of Applied Physics*, *101*(12), 123305. https://doi.org/10.1063/1.2748673

Liu, N. (2010). Model of sprite luminous trail caused by increasing streamer current. *Geophysical Research Letters*, *37*, L04102. https://doi.org/10.1029/2009GL042214

Liu, N., Pasko, V. P., Burkhardt, D. H., Frey, H. U., Mende, S. B., Su, H.-T., et al. (2006). Comparison of results from sprite streamer modeling with spectrophotometric measurements by ISUAL instrument on FORMOSAT-2 satellite. *Geophysical Research Letters*, *33*, L01101. https://doi.org/10.1029/2005GL024243

Luque, A., & Ebert, U. (2010). Sprites in varying air density: Charge conservation, glowing negative trails and changing velocity. *Geophysical Research Letters*, *37*, L06806. https://doi.org/10.1029/2009GL041982

Luque, A., Ebert, U., Montijn, C., & Hundsdorfer, W. (2007). Photoionization in negative streamers: Fast computations and two propagation modes. *Applied Physics Letters*, *90*(8), 81501. https://doi.org/10.1063/1.2435934

Luque, A., González, M., & Gordillo-Vázquez, F. J. (2017). Streamer discharges as advancing imperfect conductors: Inhomogeneities in long ionized channels. *Plasma Sources Science and Technology*, *26*(12), 125006. https://doi.org/10.1088/1361-6595/aa987a

Luque, A., Stenbaek-Nielsen, H., McHarg, M., & Haaland, R. (2016). Sprite beads and glows arising from the attachment instability in streamer channels. *Journal of Geophysical Research: Space Physics*, *121*, 2431–2449. https://doi.org/10.1002/2015JA022234

Malagón-Romero, A., & Luque, A. (2018). A domain-decomposition method to implement electrostatic free boundary conditions in the radial direction for electric discharges. *Computer Physics Communications*, *225*(114). https://doi.org/10.1016/j.cpc.2018.01.003

Morrill, J., Bucsela, E., Siefring, C., Heavner, M., Berg, S., Moudry, D., et al. (2002). Electron energy and electric field estimates in sprites derived from ionized and neutral N_2 emissions. *Geophysical Research Letters*, *29*(10), 1462. https://doi.org/10.1029/2001GL014018

Naidis, G. V. (2009). Positive and negative streamers in air: Velocity-diameter relation. *Physical Review E*, *79*(5), 57401. https://doi.org/10.1103/PhysRevE.79.057401

Obrusnik, A., Bílek, P., Hoder, T., Šimek, M., & Bonaventura, Z. (2018). Electric field determination in air plasmas from intensity ratio of nitrogen spectral bands: I. Sensitivity analysis and uncertainty quantification for dominant processes. *Plasma Sources Science and Technology*, *27*(8), 85013.

Paris, P., Aints, M., Laan, M., & Valk, F. (2004). Measurement of intensity ratio of nitrogen bands as a function of field strength. *Journal of Physics D: Applied Physics*, *37*(8), 1179. https://doi.org/10.1088/0022-3727/37/8/005

Paris, P., Aints, M., Valk, F., Plank, T., Haljaste, A., Kozlov, K. V., & Wagner, H.-E. (2005). Intensity ratio of spectral bands of nitrogen as a measure of electric field strength in plasmas. *Journal of Physics D*, *38*, 3894. https://doi.org/10.1088/0022-3727/38/21/010

Parra-Rojas, F. C., Luque, A., & Gordillo-Vázquez, F. J. (2014). Chemical and thermal impacts of sprite streamers in the Earth's mesosphere. *Journal of Geophysical Research: Space Physics*, *120*, 8899. https://doi.org/10.1002/2014JA020933

Pasko, V. P. (2010). Recent advances in theory of transient luminous events. *Journal of Geophysical Research*, *115*, A00E35. https://doi.org/10.1029/2009JA014860

Pasko, V. P., Inan, U. S., & Bell, T. F. (1996). Sprites as luminous columns of ionization produced by quasi-electrostatic thundercloud fields. *Geophysical Research Letters*, *23*, 649. https://doi.org/10.1029/96GL00473

Pasko, V. P., Yair, Y., & Kuo, C.-L. (2012). Lightning related transient luminous events at high altitude in the Earth's atmosphere: Phenomenology, mechanisms and effects. *Space Science Reviews*, *168*, 475–516. https://doi.org/10.1007/s11214-011-9813-9

Pérez-Invernón, F. J., Luque, A., & Gordillo-Vázquez, F. J. (2018). Modeling the chemical impact and the optical emissions produced by lightning-induced electromagnetic fields in the upper atmosphere: The case of halos and elves triggered by different lightning discharges. *Journal of Geophysical Research: Atmospheres*, *123*, 7615–7641. https://doi.org/10.1029/2017JD028235

Pérez-Invernón, F. J., Luque, A., Gordillo-Vazquez, F. J., Sato, M., Ushio, T., Adachi, T., & Chen, A. B. (2018). Spectroscopic diagnostic of halos and elves detected from space-based photometers. *Journal of Geophysical Research: Atmospheres*, *123*, 12,917–12,941. https://doi.org/10.1029/2018JD029053

Phelps, A. V., & Pitchford, L. C. (1985). Anisotropic scattering of electrons by N2 and its effect on electron transport. *Physical Review A*, *31*, 2932. https://doi.org/10.1103/PhysRevA.31.2932

Shcherbakov, Y. V., & Sigmond, R. (2007). Subnanosecond spectral diagnostics of streamer discharges: I. Basic experimental results. *Journal of Physics D: Applied Physics*, *40*(2), 460.

Stenbaek-Nielsen, H. C., Haaland, R., McHarg, M. G., Hensley, B. A., & Kanmae, T. (2010). Sprite initiation altitude measured by triangulation. *Journal of Geophysical Research*, *115*, A00E12. https://doi.org/10.1029/2009JA014543

Stenbaek-Nielsen, H. C., & McHarg, M. G. (2008). High time-resolution sprite imaging: Observations and implications. *Journal of Physics D*, *41*(23), 234009. https://doi.org/10.1088/0022-3727/41/23/234009

Stenbaek-Nielsen, H. C., Moudry, D. R., Wescott, E. M., Sentman, D. D., & Saõ Sabbas, F. T. (2000). Sprites and possible mesospheric effects. *Geophysical Research Letters*, *27*, 3829. https://doi.org/10.1029/2000GL003827

Stritzke, P., Sander, I., & Raether, H. (1977). Spatial and temporal spectroscopy of a streamer discharge in nitrogen. *Journal of Physics D: Applied Physics*, *10*(16), 2285.

Wescott, E. M., Sentman, D. D., Heavner, M. J., Hampton, D. L., Osborne, D. L., & Vaughan, O. H. (1996). Blue starters: Brief upward discharges from an intense Arkansas thunderstorm. *Geophysical Research Letters*, *23*, 2153. https://doi.org/10.1029/96GL01969

Wescott, E. M., Sentman, D. D., Heavner, M. J., Hampton, D. L., & Vaughan, O. H. (1998). Blue Jets: Their relationship to lightning and very large hailfall, and their physical mechanisms for their production. *Journal of Atmospheric and Solar-Terrestrial Physics*, *60*, 713. https://doi.org/10.1016/S1364-6826(98)00018-2

Wescott, E. M., Sentman, D., Osborne, D., Hampton, D., & Heavner, M. (1995). Preliminary results from the Sprites94 aircraft campaign: 2. Blue jets. *Geophysical Research Letters*, *22*, 1209. https://doi.org/10.1029/95GL00582

Wescott, E. M., Sentman, D. D., Stenbaek-Nielsen, H. C., Huet, P., Heavner, M. J., & Moudry, D. R. (2001). New evidence for the brightness and ionization of blue starters and blue jets. *Journal of Geophysical Research*, *106*, 21549. https://doi.org/10.1029/2000JA000429

Šimek, M. (2014). Optical diagnostics of streamer discharges in atmospheric gases. *Journal of Physics D: Applied Physics*, *47*(46), 463001.